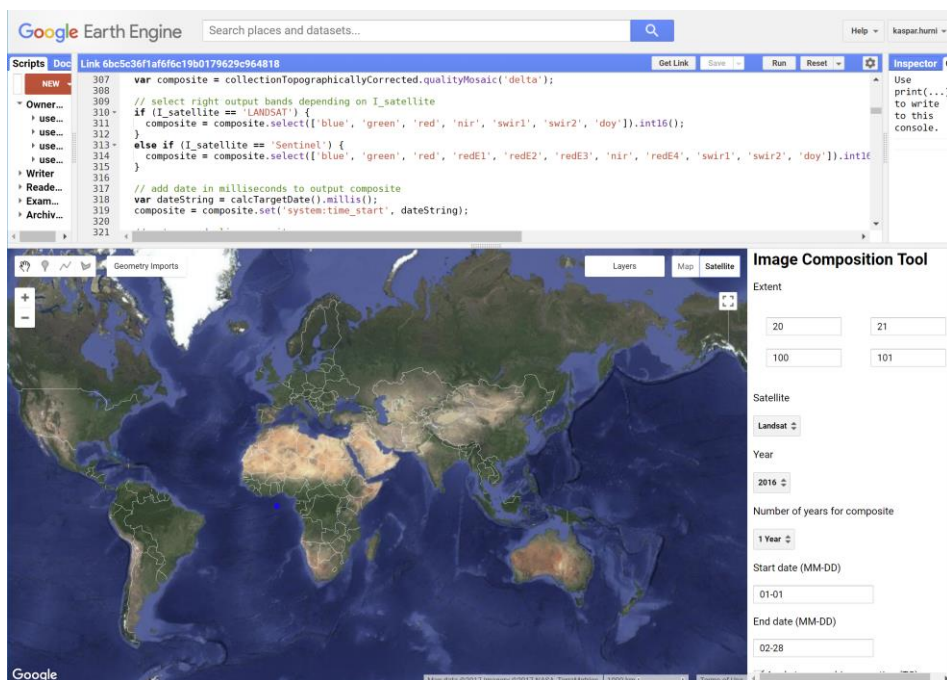# Google Earth Engine Image Pre-processing Tool:

Background and Methods

Kaspar Hurni, Andreas Heinimann, and Lukas Würsch

Centre for Development and Environment (CDE)
University of Bern

2017

Introduction

When using remote sensing data several pre-processing steps can be applied that aim at removing artefacts from the images that are not related to the actual reflectance of the land cover (e.g. sensor effects, atmospheric, and illumination conditions) (Young et al. 2017). However, the required pre-processing steps applied to the images also depend heavily on the intended use of the data. When e.g. performing a sample-based classification of individual scenes or a temporal stack of scenes within a footprint, several pre-processing steps may be skipped because training and classification are performed within the same domain (i.e. they are based on exactly the same data). This is different for e.g. trend detection algorithms, classifications across several footprints, or the classification of composite images. For such applications, a rigorous pre-processing is required so that land cover reflectance can be compared across footprints and/or time. This allows that e.g. land cover trends are extracted in an unsupervised manner or training and classification are not required to be in the same domain (i.e. classification samples collected on one image may be applied to another image) (Young et al. 2017).

In this document we present the methodological background of an image composition tool, fully implemented in Google Earth Engine (GEE). Image composition refers to an approach that creates a single, cloud-free image composite by selecting for each pixel location the best pixel from a time-series of multiple images. The combination of data from multiple images, however, requires that several pre-processing steps are applied to these images prior to the image composition. Figure 1 shows the sequential workflow of the required pre-processing steps.

Figure 1: Sequential workflow of potential pre-processing steps, adapted from (Young et al. 2017).
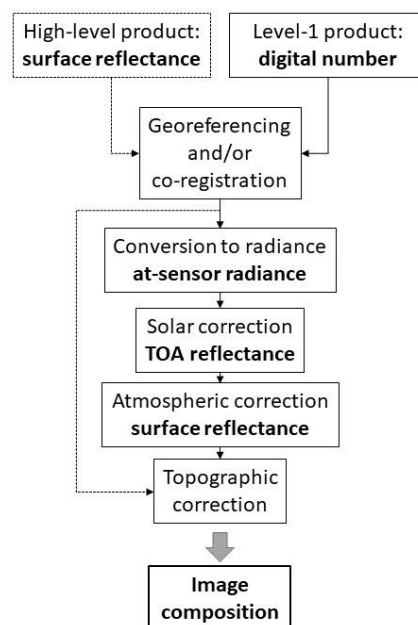
The remote sensing data, provided as level 1 product and the band values being digital numbers (DN), first needs to be georeferenced and/or co-registered so that pixel locations from one image to the other correspond (geometric correction). Next, several steps for an absolute correction are required so that we obtain the surface reflectance, which already allows a comparison across images. These steps include conversion to radiance to obtain at-sensor radiance, solar correction that results in the top of atmosphere (TOA) reflectance, and the atmospheric correction that

provides surface reflectance (SR). For Landsat, standardized pre-processing routines to obtain SR products have already been established (cf https://landsat.usgs.gov/landsat-surface-reflectance-data-products) while Sentinel SR products (referred to as "bottom of atmosphere" (BOA) reflectance by ESA) as well as harmonized Sentinel/Landsat SR (or BOA reflectance) products (cf https://earth.esa.int/web/sppa/meetings-workshops/acix) can be expected in the near future.

When performing an image composition using these standardized products, several pre-processing can thus be skipped and focus can be laid on the steps that follow, i.e. the topographic illumination correction and the image composition strategy. For these two steps, a variety of approaches and methods exist and the most appropriate pre-processing routine depends on study area and focus. For example, topographic illumination correction should be performed in a mountainous study area, but in regions with moderate terrain, this step may not be required. Furthermore, different topographic illumination correction approaches exist and their performance varies depending on the context. Some methods perform better in steep, vegetated areas, while other approaches are computationally more efficient, but are more suitable for regions with moderate terrain and/or limited vegetative cover (Teillet, Guindon, and Goodenough 1982; Riano et al. 2003). Similarly, the image composition strategy needs to be tailored to the study area and focus. For the evaluation of the "best pixel" (i.e. the pixel that is used in the composite) from a series of pixels, recent research suggests the use of multiple criteria, including scores for distance to clouds and cloud shadows, scores for each pixel reflectance in relation to the reflectance of the other pixels from the time-series, and scores for seasonal or annual variation (Hansen et al. 2008; Roy et al. 2010; Potapov, Turubanova, and Hansen 2011; Griffiths et al. 2013, 2014/8; Frantz et al. 2017). The way this scoring is performed, however, needs to be defined by the user depending on the study focus. This includes e.g. how pixel reflectance is scored (e.g. focus on low or high greenness) or the duration of the period that defines the time series of images used for the composite. Especially the last point requires flexibility, because the availability of "valid pixels" (e.g. amount of non-clouded pixels at each location) varies by region, season, and sensor revisiting period and usually needs to be evaluated for each situation.

In the following two chapters we provide the methodological background for the topographic illumination correction methods and the image composition strategies that are implemented in the GEE image pre-processing and composition tool. It provides researchers with the methodological background to optimise the image composites according to their requirements and advanced users may adjust the tool by e.g. including other topographic illumination correction methods or modifying the image composition strategy.

Topographic illumination correction

In mountain areas varying illumination conditions related to sun position, slope, and aspect result in variations of the reflectance within the same land cover type and e.g. the same forest type on a sunlit slope shows a different reflectance on a shaded slope (Riano et al. 2003). This signal-to-noise ratio can be reduced by performing a topographic illumination correction that adjusts differences in solar irradiance related to slope and aspect, resulting in an image that approximates reflectance values that would be recorded over a flat surface (Sola, González-Audícana, and Álvarez-Mozos 2016). Different approaches exist for the topographic illumination correction and they can be grouped into three categories: 1) Empirical methods, 2) physical methods, and 3) semi-empirical methods. The empirical methods do not use any additional data and derive the parameters for the topographic correction from the image, e.g. through the calculation of band ratios. However, by deriving the correction parameters through band ratios, the empirical correction methods result in the loss of spectral resolution cf (Civco 1989; Riano et al. 2003). This can reduce accuracies of e.g. multispectral classifications and therefore we did not implement any of the empirical methods in the GEE image pre-processing tool. The two other approaches additionally use a digital elevation model (DEM) for the topographic correction of the images. The DEM is used to simulate the illumination condition at the time of the image acquisition as shown in equation 1.

Equation 1: Calculation of the illumination condition (IL) for each pixel at the time of the image acquisition using a DEM, with i_s = incident angle with respect to surface normal; Z = solar zenith angle (incident angle for a horizontal surface, provided by the sensor metadata); s = terrain slope calculated from the DEM; a = solar azimuth (provided by the sensor metadata); a' = terrain aspect (azimuth) calculated from the DEM

$$IL = cos(i_s) = cos(Z) \cdot cos(s) + sin(Z) \cdot sin(s) \cdot cos(a - a')$$

The physical methods model the full path of radiance through the atmosphere to the target object and backwards and do not derive any correction parameters from the image (Sola, González-Audícana, and Álvarez-Mozos 2016). This makes the physical methods computationally efficient, but they only consider the incidence angles and do not account for diffuse irradiance, which tends to increase with increasing slope and vegetation. Physical methods therefore often result in the overcorrection of steep and vegetated areas (Teillet, Guindon, and Goodenough 1982; Meyer et al. 1993). The semi-empirical methods overcome these issues by using a DEM and by deriving correction parameters through a linear regression between each image band and the illumination condition (IL or $cos(i_s)$). This correction approach gives the correction parameters a physical meaning and the semi-empirical methods were found to outperform the other methods in the majority of studies (Sola, González-Audícana, and Álvarez-Mozos 2016). Furthermore, the semi-empirical correction can also be performed in land cover strata, which increases the quality of the corrected image even more (i.e. correction parameters are adjusted for different vegetation types and their specific diffuse irradiance) (Sola, Gonzalez-Audicana, and Alvarez-Mozos 2016). The physical and semi-empirical methods thus both have their benefits. On the one hand computational efficiency, but only for areas with moderate slopes (physical methods) and on the other hand computationally intensive, but with the ability of achieving a good correction even in steep and vegetated areas (semi-empirical methods). In the image composition tool we thus implemented both, a physical and a semi-empirical topographic illumination correction approach. We considered a large range of topographic illumination correction articles and also performed our own assessments to identify the best performing physical and semi-empirical methods from the vast range of topographic illumination correction methods. Finally, we chose to work with the Dymond-Shepherd

correction (physical) and the Statistical-Empirical correction (semi-empirical) (Dymond and Shepherd 1999; Teillet, Guindon, and Goodenough 1982).

We found that the Dymond Shepherd (D-S) correction, in contrast to the other physical methods, performs a moderate correction and does not result in very strong overcorrection of steep and vegetated slopes. This is, as shown in equation 1, because the D-S correction specifically considers incidence and exitance angles of reflectance (but still not diffuse reflectance).

Equation 1: Dymond-Shepherd topographic correction with ρ being the reflectance on a horizontal surface, ρ_s the uncorrected reflectance. Incidence and exitance angles on the level surface are i and e and on an inclined surface i_s and e_s (Dymond and Shepherd 1999).

$$\rho = \rho_s \cdot \frac{\cos(i) + \cos(e)}{\cos(i_s) + \cos(e_s)}$$

By assuming a view angle of zero (nadir) for the Landsat and Sentinel sensors, the parameters for the D-S correction can be derived from a DEM and the sensor metadata. e equals the view angle of the sensor (i.e. 0), i equals the solar zenith angle, $\cos(i_s)$ can be calculated using equation 1, and e_s equals the slope when the view angle is zero.

The Statistical-Empirical correction (semi-empirical method) was found to outperform other topographic correction approaches by the majority of the publications. We thus implemented the Stastical-Empirical correction in the tool (see equation 2) and perform the topographic correction in land cover strata.

Equation 2: Statistical-Empirical topographic illumination correction with wavelength and land cover dependent correction parameters. $\rho_{\lambda,j}$ is the corrected reflectance for wavelength λ and land cover stratum j; $\rho_{s,\lambda,j}$ is the uncorrected reflectance for wavelength λ and land cover stratum j; $\underline{\rho_{s,\lambda,j}}$ is the average uncorrected reflectance of the wavelength λ in land cover stratum j; $\cos(i_s)$ is the illumination condition (see equation 1); and $b_{\lambda,j}$ and $m_{\lambda,j}$m are the intercept and slope of the linear regression between $\cos(i_s)$ and wavelength λ in land cover stratum j (Teillet, Guindon, and Goodenough 1982).

$$\rho_{\lambda,j} = \rho_{s,\lambda,j} - \left(b_{\lambda,j} + m_{\lambda,j} \cdot \cos(i_s) \right) + \underline{\rho_{s,\lambda,j}}$$

The wavelength and land cover dependent correction parameters (intercept $b_{\lambda,j}$ and slope $m_{\lambda,j}$) are derived from the linear regression between the illumination condition and each band/wavelength within the land cover stratum using equation 3.

Equation 3: linear regression between the illumination condition ($\cos(i_s)$) and wavelength λ in land cover stratum j (Teillet, Guindon, and Goodenough 1982).

$$\rho_{s,\lambda,j} = b_{\lambda,j} + m_{\lambda,j} \cdot \cos(i_s)$$

To apply equations 2 and 3 and obtain the correction parameters, a number of pre-processing steps are required. In the tool the S-E topographic correction has thus been implemented the following way:

1) Topographic correction using the Dymond-Shepherd approach
2) Unsupervised classification of the Landsat image into 5 classes
3) Deriving of correction parameters for each wavelength and each land cover stratum
4) Applying the correction parameters to the uncorrected image

Point 1 has already been discussed above and point 2 performs an unsupervised classification using the k means algorithm (ee.Clusterer.wekaKMeans) in Google Earth Engine to obtain land cover strata (cf (Arthur and Vassilvitskii 2007)). The unsupervised classification is performed using all image bands, three tasseled cap bands (brightness, greenness, and wetness), the tasseled cap angle (Crist 1985; Powell et al. 2010), the normalized difference vegetation index (NDVI), and the normalized burn ratio (NBR). The first two points are only used to obtain a land cover classification and the image with tasseled cap bands and the D-S topographic correction applied is not further used. Using these land cover strata, the parameters for the S-E topographic correction are derived using equation 3 and applied to the image using equation 2.

Image composition

Image composition refers to an approach where a new, composite image is created using pixels from multiple images. With Landsat data such approaches became increasingly popular when the Landsat 7 data became affected by the Scan Line Corrector (SLC) failure in 2003. Initial approaches selected a clear image with leaf-on condition and then filled the SLC gaps using pixels from scenes acquired within one or two 16-day cycles (Gutman et al. 2008). Soon fully pixel-based approaches followed (i.e. without using a base image) and the composition strategies vary depending on the study focus. Recent approaches apply multiple criteria to select the best pixel from the series of available pixels, including comparisons of pixel reflectances, distance to clouds and cloud shadows, distance to the season greenness peak or the target day of the composite, and weights for different years in case the composition period spans over multiple years (Hansen et al. 2008; Roy et al. 2010; Potapov, Turubanova, and Hansen 2011; Griffiths et al. 2013; Frantz et al. 2017). The image composition strategy we implemented in the tool applies such criteria according to user defined inputs (e.g. target year, length of the season) and provides users with the flexibility to adjust the image composition to the needs of their study (e.g. focus on low or high greenness). The four criteria we implemented are described in the following sections.
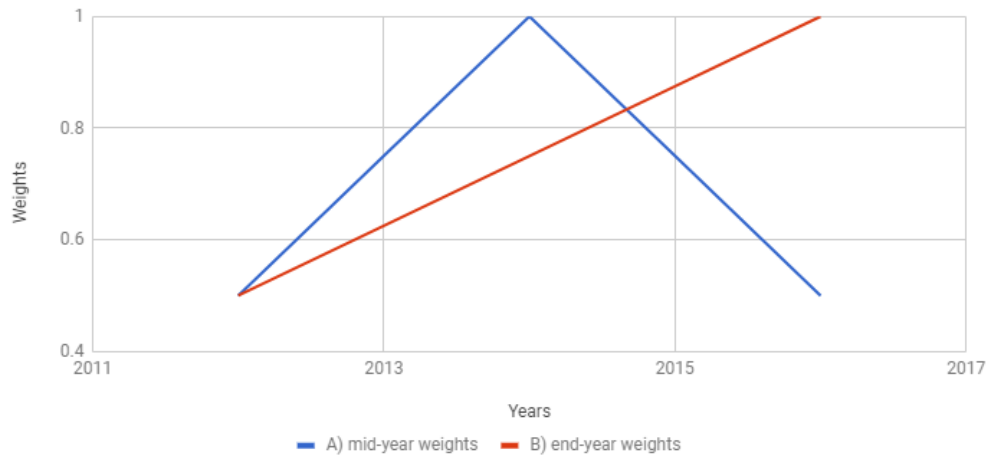
Image composition years

Usually the image composition is performed for a specific season (e.g. 2-4 months) within one year to avoid that the image composite is affected by phenology (i.e. seasonal variation of the land cover types). In heavily clouded regions, however, the composite image may be affected by no data gaps because some locations show persistent cloud cover throughout the selected season. Such composites can be improved by including images from the same season of the previous (or following) years. This minimizes "no data" gaps in the composite as well as phenology, but at the same time the composite may be affected by land cover changes that occurred over the selected years. The appropriate composition strategy thus depends on study region and focus. In the tool users can define the amount of years used for the composite (one to multiple consecutive years) and when working with multiple years they can also select which years are prioritized in the composite. A) Focus on the middle year of the composite (i.e. highest weights assigned to the "average year" of the composition period); and B) focus on the most recent year (i.e. highest weight assigned to the last year of the composition period) (see equations 4A and 4B respectively). The minimum weight we assign is 0.5 so that other parameters that consider the pixels reflectance quality (e.g. distance to clouds, pixel reflectances) have more importance in determining the ultimate weight of a pixel (see Figure 2).

Equations 4A and 4B: Calculation of pixel-based image composition weights in relation to the image acquisition years. startYear = first year considered for the composite; compYears = consecutive years to be considered in the composite; midYear = startYear + (compYears/2); acqYear = the acquisition year of a pixel; deltaYear = weight assigned to the pixel.

$$deltaYear_A = \left| \frac{|midYear - acqYear|}{compYears} - 1 \right|$$

$$deltaYear_B = \frac{acqYear - startYear}{2 \cdot compYears} + 0.5$$

Figure 2: Image composition: Weights by year. Weights are assigned to the data based on a target year (composition strategy A or B). In the illustrated example startYear = 2012 and compYears = 5 (endYear = 2016).


Image composition period

The duration of the image composition period has probably most impact on the quality of the composite, because the period defines how many images are considered for the composite. A short period may result in the occurrence of data gaps while a long period increases the amount of valid data, but may result in visible changes in phenology. To minimize this issue, images acquired mid-season (i.e. the target day) are assigned the highest weight and weights decrease towards the beginning and end of the season in a bell-shaped curve using an approximation of the Gaussian function (Equation 5 and Figure 3) (Griffiths et al. 2013).

Equation 5: Approximation of the Gaussian function to assign seasonal weights with x: acquisition day of the pixel/image; b: position of the center peak (i.e. the target day mid-season); c: standard deviation which we approximated by calculating $(endDay - startDay) \cdot 0.3$ (with a range of consecutive values the standard deviation varies with the length of the range and not its values).

$$deltaDay = e^{-\frac{(x-b)^2}{2c^2}}$$

Figure 3: Image composition: Weights by period. Weights are assigned to the data based on the period/season and the target day (mid-season), which obtains the highest weight. The example shows a start day of 170 (day of the year), end day of 250, and a target day of 210.
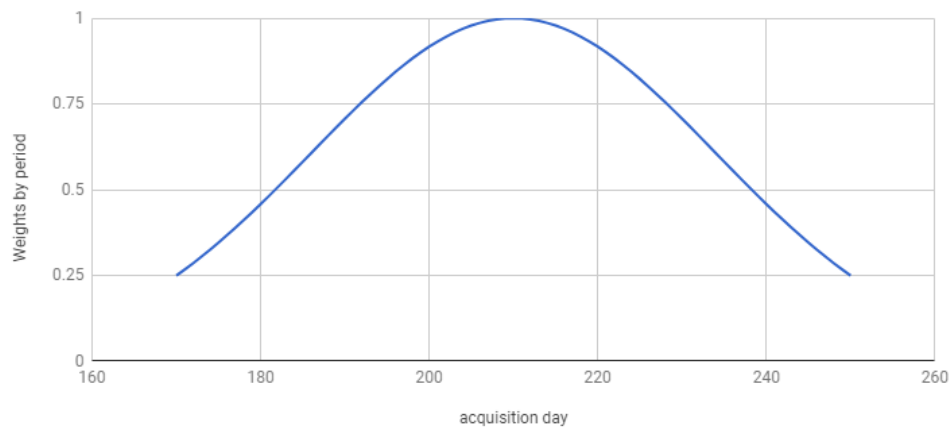
Distance to clouds and cloud shadows

Masking of clouds and cloud shadows was based on the "pixel quality attributes" band (Landsat, produced using CFMASK,
cf https://code.earthengine.google.com/dataset/LANDSAT/LC08/C01/T1_SR) or the "QA60" band (Sentinel, bit mask band with cloud mask information,
cf https://code.earthengine.google.com/dataset/COPERNICUS/S2). For Landsat we masked "cloud shadows" (bit 3), "clouds" (bit 5), medium-high "cloud confidence" (bits 6-7), and medium to high "cirrus confidence" (Landsat 8 only, bits 8-9). For Sentinel we masked "opaque" and "cirrus" pixels (bits 10 and 11 of the QA60 band) and expanded the masks by 1200m to exclude cloud edges from the images. This was not necessary for the Landsat masks, the CFMASK algorithm already masked cloud edges properly. Next, we ran a cost distance function on the data to define the distance to clouds for all unclouded pixels and assigned weights to the unclouded pixels based on their distance to clouds using the sigmoid function. This s-shaped curve gives full weight to unclouded pixels with a distance of >= 1500m to clouds and the weights decrease according to the sigmoid function the closer the pixel is to the clouds/cloud shadows (Griffiths et al. 2013, 2014/8).

Equation 6: Modified sigmoid function to assign each pixel with a weight that accounts for the distance of the pixel to clouds and cloud shadows. CloudDistance is the distance (in meters) to clouds and cloud shadows of the respective pixel.

$$cDistWeight = \frac{1}{1 + e^{(-0.008 \cdot (cloudDistance - 750))}}$$

Figure 4: Image composition: Distance to clouds weights. Weights are assigned to the pixels to account for the proximity of clouds and cloud shadows using a modification of the Sigmoid function. Pixels with a distance >1500m from clouds obtain a weight of 1.
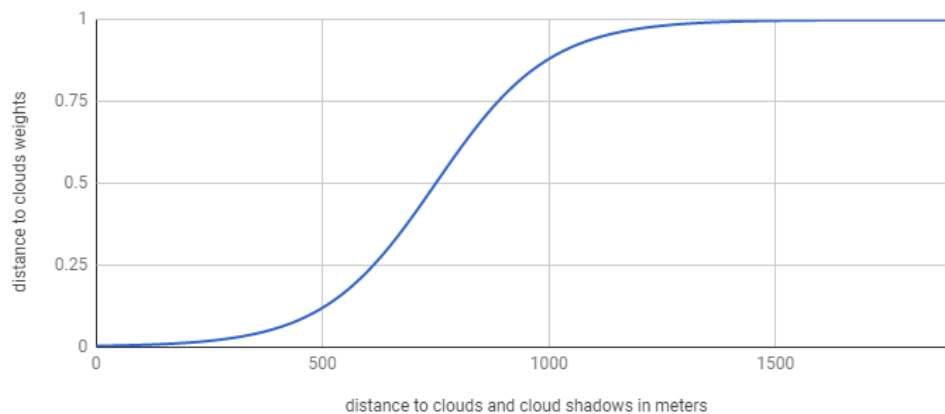
Pixel reflectance

The assessment of the pixel reflectance is performed to avoid that oversaturated, clouded, or shadowed pixels that were omitted in the cloud masking are included in the image composite. We performed this assessment on the topographically corrected near infrared (NIR) band as it shows the least noise over forested areas (cf. (Potapov, Turubanova, and Hansen 2011)) and assess for each pixel location the mean, median, minimum, maximum, and standard deviation of all valid pixels. We then provide the user with three options of assigning pixel weights:

A) The pixel with the median value obtains the highest weight and the pixel with the largest absolute deviation from the median (derived from the minimum and maximum) obtains the lowest weight. Weights for the other pixels are assigned in a linear way.

B) Focus on low greenness to obtain a composite that represents the driest status of vegetation. In this case the highest weight is assigned to the pixel closest to the 'mean reflectance minus the standard deviation'. The pixel with the largest absolute deviation from the 'mean minus standard deviation' is assigned the lowest weight and pixels in between are again assigned weights in a linear way

C) Focus on high greenness to obtain a composite that represent the most humid status of vegetation. Highest weight is assigned to the pixel closest to the 'mean plus the standard deviation', the pixel with the largest absolute deviation is assigned the lowest weight, and the other pixels obtain weights in a linear way.

Equation 7: Calculation of pixel reflectance weights using a target reflectance value. maxDif is the maximum absolute difference of all available pixels from the target reflectance value and pixDif is the absolute deviation of the considered pixel from the target reflectance value. The target reflectance value is: A) the median of all available pixels (default); B) the 'mean minus standard deviation' of all available pixels ("lower"); and C) the 'mean plus standard deviation' of all available pixels ("upper").

$$reflectanceDelta = 1 - \left(\frac{pixDif - maxDif}{maxDif} + 1 \right)$$

The most appropriate strategy needs to be evaluated by the user, as results vary by period, study region, study focus, etc. Strategy A works well in most cases, while B may include more shadowed pixels in the composite, but less clouds. Strategy C may include less shadowed pixels in the composite, but more clouds, in case some clouds/cloud shadows were not masked.

The final image composition is then performed by calculating the arithmetic mean of all four weights and the pixel with the highest weight is used for the composite.

Limitations

- Sentinel: no surface reflectance available in GEE. Until this is available the image composition using Sentinel data is performed without topographic correction. Please be careful when working with Sentinel composites as the pre-processing level of Sentinel is not yet fully suitable for all applications using image composites.

- Semi-empirical methods: computationally demanding due to the calculation of regressions. Large areas and/or long periods will most likely result in a time-out (GEE error message).

References

Arthur, David, and Sergei Vassilvitskii. 2007. "K-Means++: The Advantages of Careful Seeding." In *Proceedings of the Eighteenth Annual ACM-SIAM Symposium on Discrete Algorithms*, 1027–35. Society for Industrial and Applied Mathematics.

Civco, D. L. 1989. "TOPOGRAPHIC NORMALIZATION OF LANDSAT THEMATIC MAPPER DIGITAL IMAGERY." *Photogrammetric Engineering and Remote Sensing* 55 (9): 1303–9.

Crist, Eric P. 1985. "A TM Tasseled Cap Equivalent Transformation for Reflectance Factor Data." *Remote Sensing of Environment* 17 (3): 301–6.

Dymond, J. R., and J. D. Shepherd. 1999. "Correction of the Topographic Effect in Remote Sensing." *IEEE Transactions on Geoscience and Remote Sensing: A Publication of the IEEE Geoscience and Remote Sensing Society* 37 (5): 2618–19.

Frantz, David, Achim Röder, Marion Stellmes, and Joachim Hill. 2017. "Phenology-Adaptive Pixel-Based Compositing Using Optical Earth Observation Imagery." *Remote Sensing of Environment* 190 (March): 331–47.

Griffiths, Patrick, Tobias Kuemmerle, Matthias Baumann, Volker C. Radeloff, Ioan V. Abrudan, Juraj Lieskovsky, Catalina Munteanu, Katarzyna Ostapowicz, and Patrick Hostert. 2014. "Forest Disturbances, Forest Recovery, and Changes in Forest Types across the Carpathian Ecoregion from 1985 to 2010 Based on Landsat Image Composites." *Remote Sensing of Environment* 151: 72–88.

Griffiths, Patrick, Sebastian van der Linden, Tobias Kuemmerle, and Patrick Hostert. 2013. "A Pixel-Based Landsat Compositing Algorithm for Large Area Land Cover Mapping." *IEEE Journal of Selected Topics in Applied Earth Observations and Remote Sensing* 6 (5): 2088–2101.

Gutman, G., Raymond A. Byrnes, J. Masek, S. Covington, C. Justice, S. Franks, and Rachel Headley. 2008. "Towards Monitoring Land-Cover and Land-Use Changes at a Global Scale: The Global Land Survey 2005." *Photogrammetric Engineering and Remote Sensing* 74 (1): 6–10.

Hansen, Matthew C., David P. Roy, Erik Lindquist, Bernard Adusei, Christopher O. Justice, and Alice Altstatt. 2008. "A Method for Integrating MODIS and Landsat Data for Systematic Monitoring of Forest Cover and Change in the Congo Basin." *Remote Sensing of Environment* 112 (5): 2495–2513.

Meyer, Peter, Klaus I. Itten, Tobias Kellenberger, Stefan Sandmeier, and Ruth Sandmeier. 1993. "Radiometric Corrections of Topographically Induced Effects on Landsat TM Data in an Alpine Environment." *ISPRS Journal of Photogrammetry and Remote Sensing: Official Publication of the International Society for Photogrammetry and Remote Sensing* 48 (4): 17–28.

Potapov, Peter, Svetlana Turubanova, and Matthew C. Hansen. 2011. "Regional-Scale Boreal Forest Cover and Change Mapping Using Landsat Data Composites for European Russia." *Remote Sensing of Environment* 115 (2): 548–61.

Powell, Scott L., Warren B. Cohen, Sean P. Healey, Robert E. Kennedy, Gretchen G. Moisen, Kenneth B. Pierce, and Janet L. Ohmann. 2010. "Quantification of Live Aboveground Forest Biomass Dynamics with Landsat Time-Series and Field Inventory Data: A Comparison of Empirical Modeling Approaches." *Remote Sensing of Environment* 114 (5): 1053–68.

Riano, D., E. Chuvieco, J. Salas, and I. Aguado. 2003. "Assessment of Different Topographic Corrections in Landsat-TM Data for Mapping Vegetation Types (2003)." *IEEE Transactions on Geoscience and Remote Sensing: A Publication of the IEEE Geoscience and Remote Sensing Society* 41 (5): 1056–61.

Roy, David P., Junchang Ju, Kristi Kline, Pasquale L. Scaramuzza, Valeriy Kovalskyy, Matthew Hansen, Thomas R. Loveland, Eric Vermote, and Chunsun Zhang. 2010. "Web-Enabled Landsat Data (WELD): Landsat ETM+ Composited Mosaics of the Conterminous United States." *Remote Sensing of Environment* 114 (1): 35–49.

Sola, Ion, Maria Gonzalez-Audicana, and Jesus Alvarez-Mozos. 2016. "The Added Value of Stratified Topographic Correction of Multispectral Images." *Remote Sensing* 8 (2).

Sola, Ion, María González-Audícana, and Jesús Álvarez-Mozos. 2016. "Multi-Criteria Evaluation of Topographic Correction Methods." *Remote Sensing of Environment* 184 (October): 247–62.

Teillet, P. M., B. Guindon, and D. G. Goodenough. 1982. "On the Slope-Aspect Correction of Multispectral Scanner Data." *Canadian Journal of Remote Sensing* 8 (2): 84–106.

Young, Nicholas E., Ryan S. Anderson, Stephen M. Chignell, Anthony G. Vorster, Rick Lawrence, and Paul H. Evangelista. 2017. "A Survival Guide to Landsat Preprocessing." *Ecology* 98 (4): 920–32.